A MULTIPLICATIVE EXTENDED KALMAN FILTER FOR LOW EARTH ORBIT ATTITUDE ESTIMATION ABOARD A 0.5U SMALLSAT

Conference Paper · January 2020

CITATIONS
2

READS
384

2 authors:

Omar Awad
Draper Laboratory
2 PUBLICATIONS **2** CITATIONS
SEE PROFILE

Robert H. Bishop
University of South Florida
176 PUBLICATIONS **5,008** CITATIONS
SEE PROFILE

(Preprint) AAS 20-027

A MULTIPLICATIVE EXTENDED KALMAN FILTER FOR LOW EARTH ORBIT ATTITUDE ESTIMATION ABOARD A 0.5U SMALLSAT

Omar F. Awad* **and Robert H. Bishop†**

Attitude estimation on small satellites is much more challenging in the absence of precision sensors providing external attitude measurements, such as star trackers, sun sensors and Earth horizon sensors. Due to the size, power, and mass constraints of small satellites of with volume less than 500 cm^3 employing these precision sensors may not be practical. The proposed solution investigated here is to address the sensor deficit using a multiplicative extended Kalman filter capable of estimating attitude using a radically inexpensive inertial measurement unit, magnetometer, and the global positioning system. The key is that the computational capability of inexpensive central processing units can be utilized to host a high-fidelity magnetic field model that combined with the available measurements can be used to form a quaternion measurement processed by the multiplicative extended Kalman filter to produce a reliable attitude estimate. The results show that attitude estimates under 5 degrees of accuracy may be achievable.

INTRODUCTION

As the popularity and interest in small satellites (also known as smallsats) increases, the desire to lower the cost of the design, fabrication, and operation also increases. While inexpensive compared to larger satellites, small satellites can still be expensive to build and operate. Often a significant component of the cost, mass, and complexity is the attitude determination and control system (ADCS). Typical sensors used for attitude measurements aboard spacecraft are sun sensors, earth horizon sensors, star trackers, and even solar panels themselves. However, considering the case of small satellites, these sensors may be impractical. For purposes of this research, we consider smallsats to be in the picosatellite ($0.1 \leq m \leq 1$) to nanosatellites ($1 \leq m \leq 10$) range, where m is the spacecraft mass. The size volume that we are considering is $v \leq 500$ cm^3, where v is the volume. One of the technical challenges that guides our work is to create a *radically inexpensive* smallsat design. While there is no known consensus of what is meant by radically inexpensive, we aim for as low a cost as possible implying that expensive attitude sensors are to be avoided. At the time we began this work, our goal was to reach a $10,000 total build cost for the smallsat bus. This cost level is not easily achievable, but remains our driving goal. The total cost is, of course, correlated to the mission objectives and required payloads. We focused on an articulated communications mission operations providing thin communications across two widely separated ground stations and a small-number smallsat swarm not requiring highly accurate pointing.

A star tracker is a very effective sensor for measuring attitude and is easily capable of accuracy

*Research Assistant, Mechanical Engineering, The University of South Florida

†Professor, Electrical Engineering, The University of South Florida, 4202 E. Fowler Ave., ENB 118 Tampa, FL 33620-5350

well below 0.1°. However, star trackers can cost around \$30,000 for smallsat applications.[?,?] Earth horizon sensors can cost \$15,000 and are capable of under 0.2° of accuracy.[?] Sun sensors are much lower in cost. They can be found at approximately \$5,000 and are capable of attitude measurements of under 0.5° of accuracy.[?,?] Both Earth horizon sensors and sun sensors require that the Earth horizon and sun, respectively, are in the field of view, therefore adding pointing requirements that increase the complexity of the ADCS. All three of these sensor classes were outside the cost range of our project. Our objective was to create an attitude determination system that employed inexpensive sensors and to quantify the expected performance.

As is well-known when employing a Kalman filter architecture for state estimation there are two fundamental computational phases: the state estimate update and the state estimate propagation between the state estimate updates. During the propagation phase, we will employ an inertial measurement unit (IMU) to provide attitude rate information to enable the propagation of the attitude (as represented by an attitude quaternion) between measurements. A typical MEMS IMU is equipped with a 3-axis gyroscope, a 3-axis accelerometer, and a magnetometer and can cost less than \$30. However, MEMS IMUs are characterized by relatively large systematic errors and random noise that can cause the attitude estimation error to drift and grow over time. We use the magnetometer and an on-board model of the Earth's magnetic field to generate a *measured* attitude quaternion that is used to update the state estimate during the update phase. The multiplicative extended Kalman filter (MEKF) is capable of incorporating measures of the IMU systematic errors leading to a much improved state estimate accuracy of position, velocity, and attitude. The key to success of this approach is that the computational capability of modern processors and advanced software is sufficient to support the requisite computations. Fortunately, the cost, size, and power requirements of modern processors makes them viable for use on smallsats. One trade-off is that the low-cost processors are generally not radiation resistant.

The MEKF is a recursive *ad hoc* nonlinear filter capable of asynchronous fusion of measurements from our onboard GPS and derived quaternion measurements. Since the MEKF is a model-based architecture, modeling of the environment and sensors is important. Although nor covered here, details of our modeling approach can be found in Bishop, et al.[?] and Crain, et al.[?] Our design strategy is to include as much model complexity as possible in the initial "optimal" design and then to utilize error budgets and sensitivity analysis to systematically reduce the complexity of the MEKF while attempting to retain as close to the optimal performance as possible with tuning. In this paper we present the analysis of the MEKF and show via Monte Carlo analysis that the filter covariance does indeed reflect reality, followed by error budget and sensitivity analysis. Utilizing these results to develop a reduced-order MEKF is a topic of a future paper.

MEKF MATHEMATICAL MODELS: DYNAMICS AND SENSORS

The MEKF is model-based implying that the mathematical models of the translational and rotational dynamics of the smallsat and the mathematical models of the sensors are key to accurately estimating the state of the spacecraft. We also require mathematical models of the actuators for active control, but these are not needed for state estimation. For our smallsat application, we utilize magnetic torquers to create the attitude control torques. We do not have on-board propulsion for translational control. The MEKF timeline is illustrated in Figure **??**. During the propagation phase, we use the inertial measurement unit (IMU) to propagate the smallsat state estimate at t_{k-1}, denoted by $\hat{\mathbf{x}}_{k-1}^{+}$ to t_k, denoted by $\hat{\mathbf{x}}_{k}^{-}$. The IMU consisting of a set of accelerometers and gyros senses the linear non-gravitational acceleration and the rotational rate of the vehicle, respectively. A mathematical model of the gravity is required in the MEKF. At the measurement update, we use

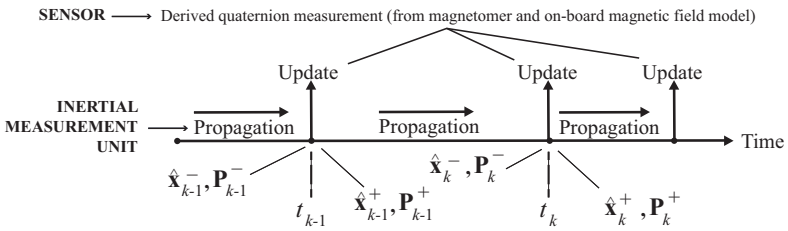

Figure 1: MEKF timeline

the GPS and a derived quaternion measurement to update the smallsat state estimate at t_k, denoted by $\hat{\mathbf{x}}_k^-$ to the state estimate after the update, denoted by $\hat{\mathbf{x}}_k^+$. The use of GPS provides measurement of position and velocity in an Earth-centered, Earth-fixed reference frame which can be transformed to Earth-centered inertial frame (here we use J2000) by a known time-varying transformation. Note that we navigate the IMU navigation base (rather than the center-of-gravity). In most MEMS IMUs, a magnetometer is paired with the IMU that measures Earth's magnetic field as a vector in the magnetometer frame (usually coincident with the IMU case frame). To utilize this measurement to derive an attitude quaternion measurement, the TRIAD algorithm is used in conjunction with an on-board model of the magnetic field.[?,?,?] We use the World Magnetic Model which is produced at regular intervals with the current model valid until 2024.[?] The derived attitude quaternion measurement, denoted by $\bar{\boldsymbol{q}}_m$, measures the attitude of the spacecraft IMU case frame (since the magnetometer is in the IMU) with respect to North-East-Down.

The state vector is comprised of the spacecraft state augmented with sensor and IMU biases and systematic errors. The state vector components are given by

$$\left.\begin{array}{l}\mathbf{r}_{imu}\\ \mathbf{v}_{imu}\\ \bar{\boldsymbol{q}}_i^b\end{array}\right\} \text{smallsat parameters} \qquad \left.\begin{array}{l}\mathbf{b}_q\\ \mathbf{b}_p\\ \mathbf{b}_v\end{array}\right\} \text{sensor biases}$$

$$\left.\begin{array}{l}\mathbf{b}_a\\ \mathbf{s}_a\\ \boldsymbol{\gamma}_a\end{array}\right\} \text{accelerometer bias/errors} \qquad \left.\begin{array}{l}\mathbf{b}_g\\ \mathbf{s}_g\\ \boldsymbol{\gamma}_g\end{array}\right\} \text{gyro bias/errors}$$

where $\mathbf{r}_{imu}(t)$ and $\mathbf{v}_{imu}(t)$ are the position and velocity, respectively, of the IMU represented in the inertial reference frame, and $\bar{\mathbf{q}}_i^b(t)$ represents the orientation of the spacecraft body fixed reference frame with respect to the inertial reference frame. Note that during the state update at t_k, we do not directly update the quaternion, but rather update the attitude error, denoted by $\delta\hat{\boldsymbol{\alpha}}_k^+$, and then the quaternion update is

$$\hat{\bar{\mathbf{q}}}_{i,k}^{b^+} = \begin{bmatrix} \frac{1}{2}\delta\hat{\boldsymbol{\alpha}}_k^+ \\ 1 \end{bmatrix} \otimes \hat{\bar{\mathbf{q}}}_{i,k}^{b^-}, \tag{1}$$

where $\hat{\bar{\mathbf{q}}}_{i,k}^{b^-}$ is the *a priori* estimate of the quaternion and $\delta\hat{\boldsymbol{\alpha}}_k^- = 0$. The quaternion in Eq. (**??**) satisfies the unity norm constraint only to first order, and so to ensure that the quaternion remains unity norm a normalization is performed. The initial state estimation error covariance for the spacecraft state, denoted by $\mathbf{P}_s \in \mathbb{R}^{9\times 9}$, is sampled to obtain the initial spacecraft state for the simulations.

The model of the IMU measurement of the non-gravitational acceleration includes errors due to nonorthogonality and misalignment of the axes, $\boldsymbol{\gamma}_a \in \mathbb{R}^6$, errors due to scale-factor uncertainties,

$\mathbf{s}_a \in \mathbb{R}^3$, random biases, $\mathbf{b}_a \in \mathbb{R}^3$, and random noise, $\boldsymbol{\eta}_a(t) \in \mathbb{R}^3$, where $\boldsymbol{\eta}_a(t)$ is a zero-mean, white noise process with covariance

$$\mathrm{E}\left\{\boldsymbol{\eta}_a(t)\boldsymbol{\eta}_a^{\mathrm{T}}(\tau)\right\} = \mathbf{Q}_a\delta(t-\tau) \in \mathbb{R}^{3\times 3}\,,$$

and $\mathbf{Q}_a = \mathbf{Q}_a^T \geq 0$. Similarly, the model of the IMU measurement of the angular velocity of the spacecraft includes errors due to nonorthogonality and misalignment of the axes, $\boldsymbol{\gamma}_g \in \mathbb{R}^6$, errors due to scale-factor uncertainties, $\mathbf{s}_g \in \mathbb{R}^3$, random biases, $\mathbf{b}_g \in \mathbb{R}^3$, and random noise, $\boldsymbol{\eta}_g(t) \in \mathbb{R}^3$ where $\boldsymbol{\eta}_g(t)$ is a zero-mean, white noise process with covariance

$$\mathrm{E}\left\{\boldsymbol{\eta}_g(t)\boldsymbol{\eta}_g^{\mathrm{T}}(\tau)\right\} = \mathbf{Q}_g\delta(t-\tau) \in \mathbb{R}^{3\times 3}\,,$$

and $\mathbf{Q}_g = \mathbf{Q}_g^T \geq 0$ is given. We model $\mathbf{b}_a$, $\boldsymbol{\gamma}_a$, $\mathbf{s}_a$, $\mathbf{b}_g$, $\boldsymbol{\gamma}_g$, and $\mathbf{s}_g$ as random constants with $\mathrm{E}\left\{\mathbf{b}_a\right\} = 0$, $\mathrm{E}\left\{\boldsymbol{\gamma}_a\right\} = 0$, $\mathrm{E}\left\{\mathbf{s}_a\right\} = 0$, $\mathrm{E}\left\{\mathbf{b}_a\mathbf{b}_a^{\mathrm{T}}\right\} = \mathbf{P}_{\mathbf{b}_a} = \mathbf{P}_{\mathbf{b}_a}^{\mathrm{T}} \in \mathbb{R}^{3\times 3}$, $\mathrm{E}\left\{\mathbf{s}_a\mathbf{s}_a^{\mathrm{T}}\right\} = \mathbf{P}_{\mathbf{s}_a} = \mathbf{P}_{\mathbf{s}_a}^{\mathrm{T}} \in \mathbb{R}^{3\times 3}$, and $\mathrm{E}\left\{\boldsymbol{\gamma}_a\boldsymbol{\gamma}_a^{\mathrm{T}}\right\} = \mathbf{P}_{\boldsymbol{\gamma}_a} = \mathbf{P}_{\boldsymbol{\gamma}_a}^{\mathrm{T}} \in \mathbb{R}^{6\times 6}$, and where $\mathbf{P}_{\mathbf{b}_a} > 0$, $\mathbf{P}_{\mathbf{s}_a} > 0$, and $\mathbf{P}_{\boldsymbol{\gamma}_a} > 0$ are given and $\mathrm{E}\left\{\mathbf{b}_g\right\} = 0$, $\mathrm{E}\left\{\boldsymbol{\gamma}_g\right\} = 0$, $\mathrm{E}\left\{\mathbf{s}_g\right\} = 0$, and $\mathrm{E}\left\{\mathbf{b}_g\mathbf{b}_g^{\mathrm{T}}\right\} = \mathbf{P}_{\mathbf{b}_g} = \mathbf{P}_{\mathbf{b}_g}^{\mathrm{T}} \in \mathbb{R}^{3\times 3}$, $\mathrm{E}\left\{\mathbf{s}_g\mathbf{s}_g^{\mathrm{T}}\right\} = \mathbf{P}_{\mathbf{s}_g} = \mathbf{P}_{\mathbf{s}_g}^{\mathrm{T}} \in \mathbb{R}^{3\times 3}$, and $\mathrm{E}\left\{\boldsymbol{\gamma}_g\boldsymbol{\gamma}_g^{\mathrm{T}}\right\} = \mathbf{P}_{\boldsymbol{\gamma}_g} = \mathbf{P}_{\boldsymbol{\gamma}_g}^{\mathrm{T}} \in \mathbb{R}^{6\times 6}$ and where $\mathbf{P}_{\mathbf{b}_g} > 0$, $\mathbf{P}_{\mathbf{s}_g} > 0$, and $\mathbf{P}_{\boldsymbol{\gamma}_g} > 0$ are given.

The derived quaternion measurement error model includes both a random bias, $\mathbf{b}_q \in \mathbb{R}^3$, and a white-noise sequence, $\boldsymbol{\eta}_{q_k} \in \mathbb{R}^3$. The bias-noise quaternion at t_k is formed as

$$\bar{\mathbf{q}}_{b,\eta_k} = \begin{bmatrix} \sin\left(\dfrac{\theta_{q_k}}{2}\right)\dfrac{\boldsymbol{\theta}_{q_k}}{\theta_{q_k}} \\ \cos\left(\dfrac{\theta_q}{2}\right) \end{bmatrix}, \tag{2}$$

where

$$\boldsymbol{\theta}_{q_k} = \mathbf{b}_q + \boldsymbol{\eta}_{q_k} \quad \text{and} \quad \theta_{q_k} = \|\boldsymbol{\theta}_{q_k}\|, \tag{3}$$

where

$$\mathrm{E}\left\{\boldsymbol{\eta}_{q_k}\boldsymbol{\eta}_{q_j}^{\mathrm{T}}\right\} = \mathbf{R}_q\delta_{kj} \in \mathbb{R}^{3\times 3}\,,$$

and $\mathbf{R}_q = \mathbf{R}_q^T > 0$ is given. We model $\mathbf{b}_q$ as a random constant vector with $\mathrm{E}\left\{\mathbf{b}_q\right\} = 0$ and $\mathrm{E}\left\{\mathbf{b}_q\mathbf{b}_b^{\mathrm{T}}\right\} = \mathbf{P}_{\mathbf{b}_q} > 0 \in \mathbb{R}^{3\times 3}$ is given. The GPS position and velocity measurement error models include biases and random noise. For the GPS position measurement at time t_k we have a random bias $\mathbf{b}_p \in \mathbb{R}^3$ and the white-noise sequence, $\boldsymbol{\eta}_{p_k} \in \mathbb{R}^3$ where

$$\mathrm{E}\left\{\boldsymbol{\eta}_{p_k}\boldsymbol{\eta}_{q_j}^{\mathrm{T}}\right\} = \mathbf{R}_p\delta_{kj} \in \mathbb{R}^{3\times 3}\,,$$

and $\mathbf{R}_p = \mathbf{R}_q^T > 0$ is given. We model $\mathbf{b}_p$ as a random constant vector with $\mathrm{E}\left\{\mathbf{b}_p\right\} = 0$ and $\mathrm{E}\left\{\mathbf{b}_p\mathbf{b}_p^{\mathrm{T}}\right\} = \mathbf{P}_{\mathbf{b}_q} > 0 \in \mathbb{R}^{3\times 3}$ is given. Similarly for the GPS velocity measurement.

In the MEKF, the initial covariance matrix, $\mathbf{P}_0 \in \mathbb{R}^{42\times 42}$, is formed using $\mathbf{P}_s$, $\mathbf{P}_{\mathbf{b}_a}$, $\mathbf{P}_{\mathbf{s}_a}$, $\mathbf{P}_{\boldsymbol{\gamma}_a}$, $\mathbf{P}_{\mathbf{b}_g}$, $\mathbf{P}_{\mathbf{s}_g}$, $\mathbf{P}_{\boldsymbol{\gamma}_g}$, $\mathbf{P}_{\mathbf{b}_q}$, $\mathbf{P}_{\mathbf{b}_p}$, and $\mathbf{P}_{\mathbf{b}_v}$. The measurement noise covariance matrix $\mathbf{R} \in \mathbb{R}^{10\times 10}$ is

formed using $\mathbf{R}_q$, $\mathbf{R}_p$, and $\mathbf{R}_v$. The process noise spectral density is formed using $\mathbf{Q}_a$ and $\mathbf{Q}_g$. Note that in the design of the MEKF, we often utilize the process noise spectral density and measurement noise covariance as tuning parameters.

RESULTS

The analysis presented here includes the results of four types of numerical simulation studies:

1. Single run simulations
2. Monte Carlo simulations
3. Error budgets
4. Sensitivity analysis

The Monte Carlo simulation studies are used to confirm that the MEKF state estimation error covariance reflects reality. This is especially important since we are using an extended Kalman filter which is known to be an *ad hoc* algorithm requiring careful tuning to obtain realistic results. The error budget analysis and associated sensitivity analysis illuminates the major sources of state estimation error resulting from various classes of uncertainty (such as measure and process noise).

The simulated orbit is circular at 400km and inclination of 28.5°. After the smallsat is deployed, we assume that it is initially tumbling about all three axis at a constant rate of 11.5°/s. It is assumed that the de-tumbling maneuver takes about 30s followed by 30s of stable motion. The simulation time is then 60s total. The GPS measurement update rate is 5Hz and the computed quaternion measurement update rate is 5Hz. The Monte Carlo analysis includes 100 runs. The filter uncertainty parameters are given in Table **??** and are defined for all runs.

Figures **??**–**??** illustrate the MEKF performance in estimating the position, velocity, and attitude of the smallsat. In each figure we present a single simulation overlayed with the results of the Monte Carlo analysis. For example, in Figure **??**, we note that the Monte Carlo results match the single run state estimation error covariance quite well indicating that the MEKF is well-tuned. Similarly for the state estimation velocity errors in Figure **??**. In Figure **??** we see that the attitude estimation errors are less than 5°. This is a first indication that the MEKF processing the derived quaternion measurement and the GPS can produce state estimates (especially attitude) that are consistent with many smallsat mission objects, requiring sun pointing, for example.

Table 1: MEKF parameter values

	Associated variable	**Description**	**Value (STD)**
Initial covariance	$\mathbf{P}_s$	Position uncertainty	4 m
		Velocity uncertainty	0.11 m/s
		Attitude uncertainty	0.1 rad
	$\mathbf{P}_{\mathbf{b}_p}$	GPS pos bias uncertainty	1 m
	$\mathbf{P}_{\mathbf{b}_v}$	GPS vel bias uncertainty	0.01 m/s
	$\mathbf{P}_{b_q}$	Derived quaternion bias	0.05 rad
	$\mathbf{P}_{\boldsymbol{\gamma}_a}$	IMU accel misalign/non-orthog	0.0032 m/s^2
	$\mathbf{P}_{\mathbf{s}_a}$	IMU accel scale factor	0.0032 m/s^2
	$\mathbf{P}_{\mathbf{b}_a}$	IMU accel bias	0.08 m/s^2
	$\mathbf{P}_{\boldsymbol{\gamma}_g}$	IMU gyro misalign/non-orthog	0.0032 rad/s
	$\mathbf{P}_{\mathbf{s}_g}$	IMU gyro scale factor	0.0032 rad/s
	$\mathbf{P}_{\mathbf{b}_g}$	IMU gyro bias	0.08 rad/s
Measurement Noise	$\mathbf{R}_p$	GPS position	3 m
	$\mathbf{R}_v$	GPS velocity	0.1 m/s
	$\mathbf{R}_q$	Derived quaternion	0.05 rad
Process Noise	$\mathbf{Q}_a\delta(t-\tau)$	IMU accel noise	0.0175 m/s^2
	$\mathbf{Q}_g\delta(t-\tau)$	IMU gyro noise	0.0175 rad/s

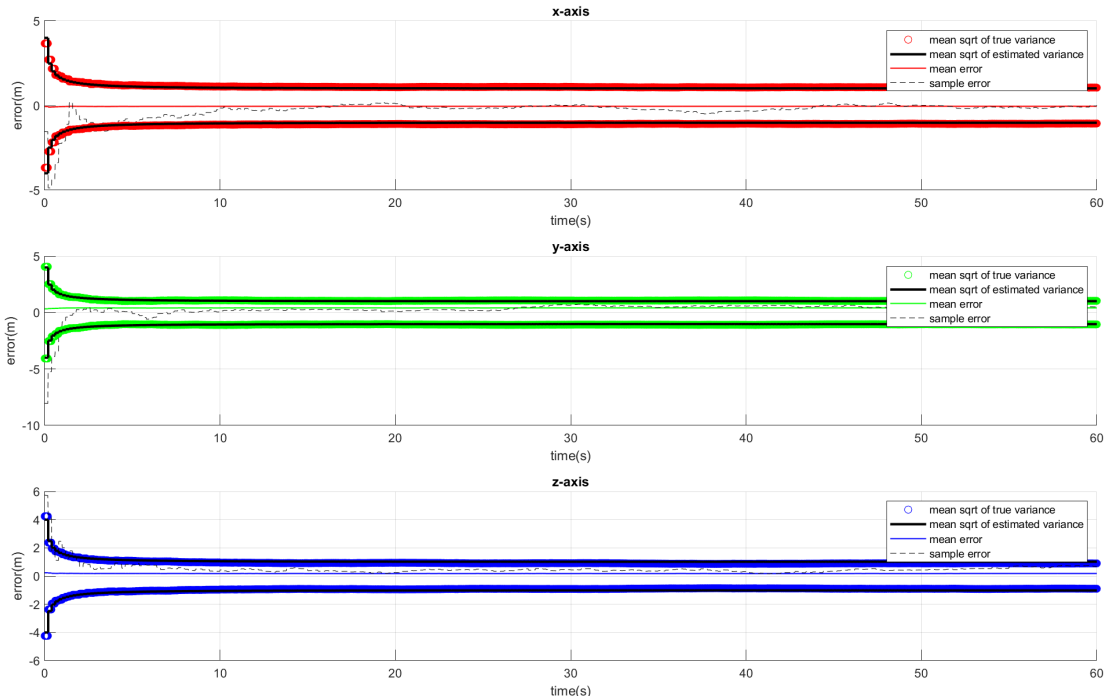

Figure 2: Position estimation

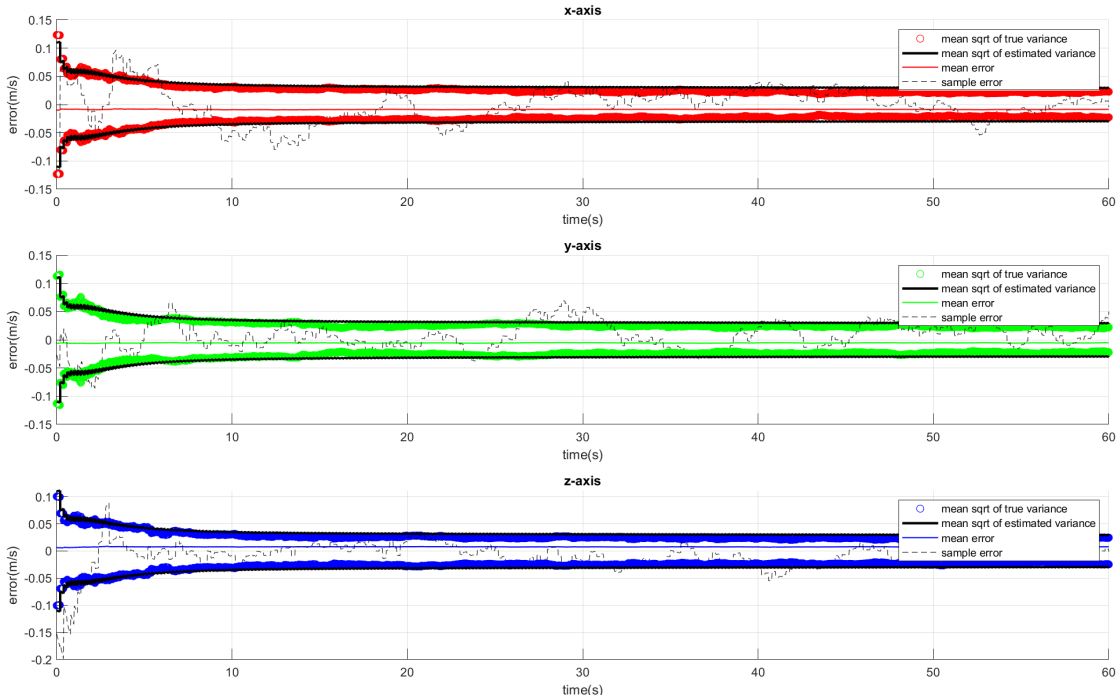

Figure 3: Velocity estimation

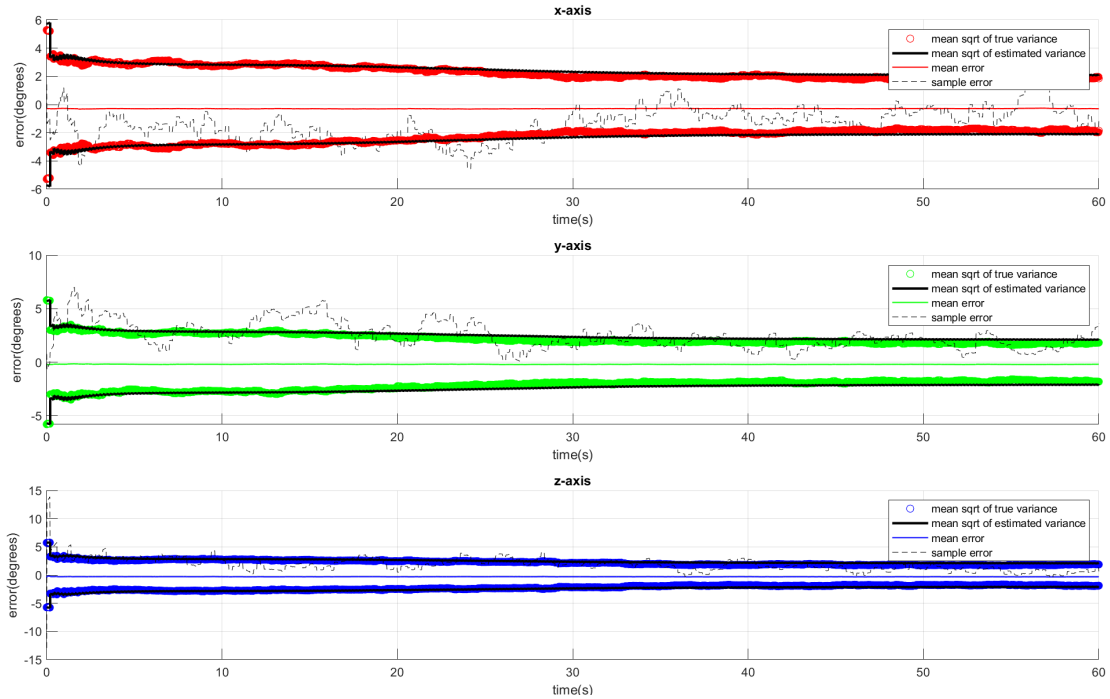

Figure 4: Attitude estimation

Error Budget

The error budget is a catalog of the effect of various uncertainties on ability of the MEKF to estimate the state accurately. This is quantified by computing the contributions of the various systematic and random errors to the overall state estimation uncertainty at some point(s) in time. Specifically, we are considering the state estimation error covariance at the end of the de-tumbling phase (at $t = 60$s). We subdivide the error sources into three main categories: initial state estimation error covariance, process noise spectral density, and measurement noise covariance. Each of these three categories may then be further subdivided to refine the error budget. The error sources/groups are listed in Table **??**.

Table 2: Error Group Designations

	Group #	**Name**
Initial Covariance	1	Position uncertainty
	2	Velocity uncertainty
	3	Attitude uncertainty
	4	GPS position measurement bias uncertainty
	5	GPS velocity measurement bias uncertainty
	6	Attitude quaternion measurement bias uncertainty
	7	Accelerometer misalignment uncertainty
	8	Accelerometer non-orthogonality uncertainty
	9	Accelerometer scaling uncertainty
	10	Accelerometer bias uncertainty
	11	Gyroscope misalignment uncertainty
	12	Gyroscope non-orthogonality uncertainty
	13	Gyroscope scaling uncertainty
	14	Gyroscope bias uncertainty
Measurement Noise	15	GPS position noise
	16	GPS velocity noise
	17	Attitude quaternion noise
Process Noise	18	Velocity process noise
	19	Attitude process noise

Table 3: Error Budget

Error Group	Pos (m)			Vel (m/s)			Att (deg)		
1	0.2419	0.242	0.2419	0.0002987	0.0002779	0.0002986	0.0005426	0.0004873	0.0004595
2	0.01319	0.01156	0.01316	0.00133	0.0003679	0.001325	0.04861	0.09285	0.0569
3	0.000377	0.000424	7.761e−5	1.745e−5	4.813e−5	2.114e−5	0.7564	1.083	0.7542
4	0.9395	0.9395	0.9395	7.468e−5	6.949e−5	7.465e−5	0.0001356	0.0001218	0.0001149
5	0.1301	0.1302	0.1301	0.008661	0.00867	0.008659	0.002867	0.006803	0.00408
6	0.0008455	0.0007051	8.006e−5	2.724e−5	0.0001298	1.853e−5	1.604	2.338	1.602
7	1.569e−7	5.257e−5	6.112e−8	4.204e−8	7.805e−7	2.116e−8	3.792e−6	1.249e−6	4.884e−6
8	1.569e−7	5.257e−5	6.112e−8	4.204e−8	7.805e−7	2.116e−8	3.792e−6	1.249e−6	4.884e−6
9	2.214e−5	7.849e−8	3.234e−5	3.256e−7	4.845e−9	2.244e−6	3.185e−6	2.828e−5	1.32e−6
10	0.00164	0.0009806	0.0005687	0.0005551	0.0005078	0.0004579	0.01631	0.0215	0.02358
11	8.14e−6	2.169e−5	1.849e−6	9.289e−7	9.043e−6	1.606e−6	0.05762	0.01025	0.05749
12	8.207e−6	2.169e−5	1.922e−6	8.856e−7	9.052e−6	1.581e−6	0.05763	0.01021	0.05751
13	7.792e−7	3.837e−7	1.312e−6	1.847e−6	1.262e−6	3.809e−7	0.008513	0.01447	0.007511
14	0.0002409	0.0001278	0.0002224	7.91e−5	6.756e−5	5.438e−5	0.1064	0.03974	0.111
15	0.2425	0.2425	0.2425	0.003711	0.003944	0.003711	0.007957	0.01186	0.006839
16	0.124	0.1249	0.124	0.02171	0.02152	0.02171	0.1222	0.1981	0.1234
17	0.0003446	0.0001947	0.0001285	9.398e−5	0.0001181	6.81e−5	1.015	0.9358	1.022
18	0.01086	0.004661	0.0108	0.01873	0.01885	0.01872	0.0904	0.1577	0.123
19	0.0002466	0.0004109	0.0001054	70.643e−5	0.0001878	7.106e−5	1.316	0.8164	1.311
RSS	1.016	1.016	1.016	0.03022	0.03016	0.03021	2.439	2.874	2.44

Sensitivity Analysis

The sensitivity analysis follows directly from the results of the error budget. The error budget was computed with static uncertainty/error values. While the error budget shows which states contribute the most towards the overall uncertainty, those contributions come from static values. Therefore, this only represents a single scenario of uncertainty. To properly analyze the effect each error group on the overall uncertainty, we must look at a range of each error group's uncertainty rather than a single point. By varying or scaling each error group's uncertainty, we can see how it affects the Kalman filter's overall estimation uncertainty. If scaling the error group's value does not change the overall uncertainty much, then the estimate is not sensitive to the error group. However, if the overall uncertainty increases significantly with the scaling of the error group, then the estimate is very sensitive to that error term. This is the final step in determining which states or error terms can be neglected to simplify the filter. If an error group is seen to have little to no impact on all three main states (position, velocity, and attitude), then we may remove it from our filter.

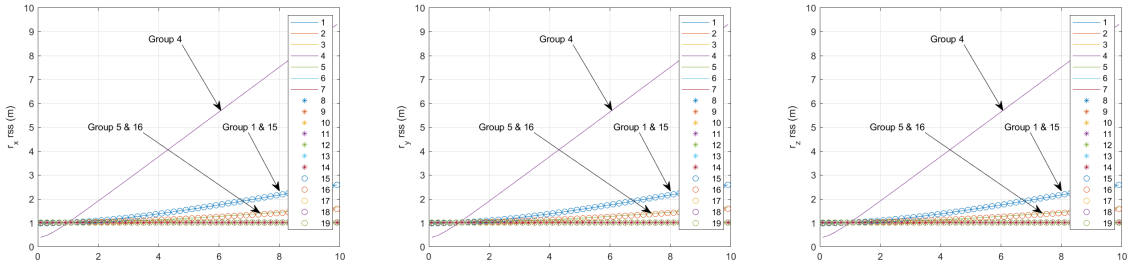

Figure 5: Position Sensitivity Analysis

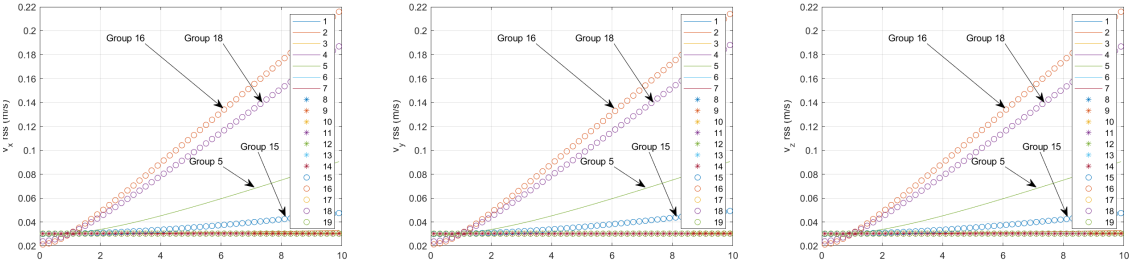

Figure 6: Velocity Sensitivity Analysis

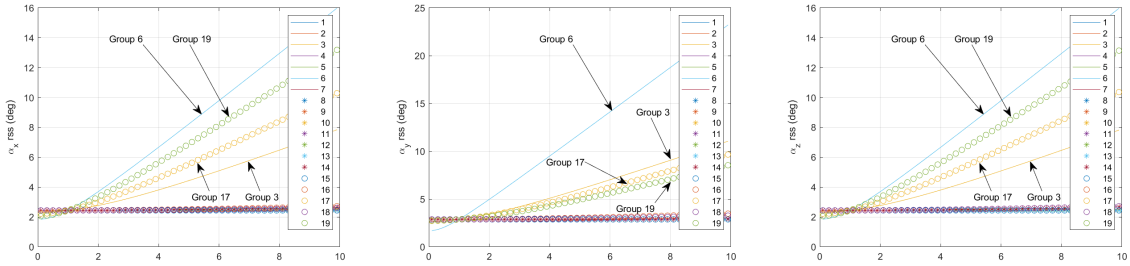

Figure 7: Attitude Sensitivity Analysis

CONCLUSIONS

The results strongly indicate that the MEKF is a viable option for smallsat state estimation using GPS in conjunction with a MEMS IMU and an on-board model of the magnetic field to produce position, velocity, and attitude estimates. The attitude estimation uncertainty on the order of 3° are achievable. This assumes that the magnetic model is accurate. The influence of uncertainties in the magnetic field model is a current area of investigation.

REFERENCES

[1] https://www.cubesatshop.com/product/kul-star-tracker/

[2] https://www.cubesatshop.com/product/mai-ss-space-sextant/

[3] https://www.cubesatshop.com/product/mai-ses-ir-earth-sensor/

[4] https://www.cubesatshop.com/product/nss-cubesat-sun-sensor/

[5] https://www.cubesatshop.com/product/nano-ssoc-a60-analog-sun-sensor/

[6] Bishop, R. H., Crain, T. P., DeMars, K. J., Hanak, C., Carson III, J. M., Trawny, N., and Christian, J. A., "An Inertial Dual-State State Estimator for Precision Planetary Landing with Hazard Detection and Avoidance," *AIAA Guidance, Navigation, and Control Conference*, AIAA SciTech, AIAA 2016-0098, San Diego, CA, 2016.

[7] Crain, T. P., Bishop, R. H., Carson III, J. M., Trawny, N., Sullivan, J., Christian, J. A., DeMars, K. J., Getchius, J., and Hanak, C., "Approach-Phase Precision Landing with Hazard Relative Navigation: Terrestrial Test Campaign Results of the Morpheus/ALHAT Project," *AIAA Guidance, Navigation, and Control Conference*, AIAA SciTech, AIAA 2016-0099, San Diego, CA, 2016.

[8] Lefferts, E., Markley, L., and and Shuster, M., "Kalman Filtering for Spacecraft Attitude Estimation," *AIAA Journal of Guidance, Control, and Dynamics*, Vol. 5, No. 5, 1982, pp. 417-429.

[9] Bar-Itzhack, I. Y. and Harman, R. R., "Optimized TRIAD Algorithm for Attitude Determination," *AIAA Journal of Guidance, Control, and Dynamics*, Vol. 20, No. 1, 1997, pp. 208-211.

[10] Natanson, G., Challa, M., Deutschmann, J., and Baker, D., "Magnetometer-only Attitude and Rate Determination for a Gyroless Spacecraft," *Proceedings of the Third International Symposium on Space Mission Operations and Ground Data Systems*, NASA Conference Publication 3281, 1994, pp. 791-798.

[11] https://www.ngdc.noaa.gov/geomag/WMM/DoDWMM.shtml